Journal of Materials Chemistry A

Accepted Manuscript

ROYAL SOCIETY OF CHEMISTRY

www.rsc.org/materialsA

Journal Name

ARTICLE

Ultrathin mesoporous Co_3O_4 nanosheets with excellent photo-/thermo-catalytic activity†

Received 00th January 20xx,
Accepted 00th January 20xx

DOI: 10.1039/x0xx00000x

www.rsc.org/

Yali Zheng,[a] Wenzhong Wang,*[a] Dong Jiang,[a] Ling Zhang,[a] Xiaoman Li[a] and Zhong Wang[a]

Ultrathin mesoporous Co_3O_4 nanosheets on stainless steel mesh (SS-Co_3O_4) have been synthesized through an electrochemistry deposition method. The SS-Co_3O_4 catalyst exhibits high photothermal performance, resulting in a considerable increase of temperature above the light-off temperature for VOCs oxidation. Aerobic oxidations of propylene and propane under simulated sunlight were selected as probe reactions to explore the photo-/thermo-catalytic (PTC) activity. The results show that SS-Co_3O_4 with only 7 mg of Co_3O_4 grown on the substrate possesses superior PTC activity, which merely occurs around the direct grown SS-Co_3O_4 rather than the Co_3O_4 coated SS. The combined properties of SS-Co_3O_4 such as ultrathin two-dimensional shape, foam-like porous inside architecture, and supported metal substrate could lead to the integrative advantages of the maximum utilization of photothermal conversion, more catalytic active sites, and enhanced amount and mobility of surface lattice oxygen species, resulting in the excellent PTC activity of SS-Co_3O_4.This work provides the insights into the rational design of monolith catalysts for the solar driven environmental purification and suggests new ideas toward the overall utilization of solar energy.

1. Introduction

The control of VOCs emissions is very important for a wide range of applications. Catalytic oxidation using transition metal oxides is considered to be one of the most efficient routes. However, high operating temperature in this process means low energy efficiencies, and will compromise the long-term stability of catalysts, decrease the selectivity for the desired products.[1] At present, the development of effective catalysts for complete oxidation of VOCs at low temperature is still a challenge to be solved.[2]

In this regard, nature has already set a good example for us. UV-Vis light of the solar spectrum with higher energy could be used to activate photocatalytic (PC) reaction, while the infrared part can supply needed endothermic energy for thermocatalytic (TC) reaction.[3] The PC conversion of solar energy to chemical energy is convenient and sustainable for chemical reactions because solar light is abundant and it can facilitate room temperature chemical transformations by generating electronically excited states in photocatalysts.[4] Meanwhile, suitable catalysts can efficiently absorb light and release the absorbed light energy in the form of heat (photothermal effect), resulting in a considerable increase of temperature, which is just enough to stimulate TC process. Therefore, integrating mild TC into PC should be promising for utilizing the solar energy and avoiding high operating temperature. Compared with sole PC and TC, photo-/thermo-catalysis (PTC) possesses following advantages: (i) the processes are characterized by high energy efficiencies without input of thermal energy; (ii) the temperature on the catalyst surface rises instantaneously due to photothermal effect,[5] and the heat is confined on the surface of the catalyst (local temperature effect);[6] (iii) the rate constant of the PTC process is much higher than a linear combination of TC and PC, which is attributed to the existence of a PTC synergetic effect;[7-9] (iv) in some cases, PTC can effectively refrain the deactivation of the catalyst[10] and increase the selectivity for the desired products. Recently, we proposed an integration of solar energy conversion with synergistic low-temperature catalysis in $Ce_{1-x}Bi_xO_{2-\delta}$ nanorods, the coupled electronic and ionic conduction help improve the negative temperature effect and integrate synergistic low temperature catalysis into solar energy utilization.[11]

In most cases, the catalysts are used in the form of powder or supported on cordierite, which will not be helpful for the maximum utilization of the photothermal effect and will sacrifice the overall activity. Therefore, how to prepare supported catalysts with high efficiency for the photothermal utilization is particularly important, which is another issue to be considered. Metal substrate such as stainless steel mesh (SS) supported catalysts come to mind because they can realize much stronger photoabsorption abilities than traditional catalysts and display a strong photothermal effect.

[a] State Key Laboratory of High Performance Ceramics and Superfine Microstructures, Shanghai Institute of Ceramics, Chinese Academy of Sciences, 1295 Dingxi Road, Shanghai 200050, P. R. China. E-mail: wzwang@mail.sic.ac.cn

†Electronic Supplementary Information (ESI) available: [Co_3O_4-O preparation,, electrophoresis of SS-Co_3O_4 (EP), electrochemical analysis, and TG/DTA analysis. Fig. S1-S10 displayed the XRD patterns, UV-Vis-IR spectra, TEM images, N_2 adsorption-desorption isotherm, pore size distributions, temporal change of the temperature under Xe irradiation, blank experiments for C_3H_6 and C_3H_8 oxidation, consecutive cyclic tests and current–time curves of the samples.]. See DOI: 10.1039/x0xx00000x

The use of metal substrate has a number of advantages. First, high heating rate can be expected due to the low heat capacity of the metal substrate, it is much more easily to achieve the light-off temperature of the catalyst. Second, with good thermal conductivity and fast heat transfer property, the metal substrate can effectively prevent the overheating induced deactivation of the catalyst. The catalyst can quickly achieve uniform temperature because of the high mass and heat transfer coefficient. Besides, research has shown that for stainless steel nets used as supports of dye-doped mesostructured films, the tiny grids of them could be regarded as laser resonant structures for feedback of light.[12] Taken together, above effects can allow significant photothermal heating of the catalyst with surprisingly small amounts of optical energy input.[13] Co_3O_4 has been reported to be the most active in VOCs catalytic combustion.[14, 15] As certified photocatalyst and universal thermocatalyst, Co_3O_4 can be expected to show high PTC activity. Studies have shown that freestanding Co_3O_4 nanosheets on conductive substrate could expose the maximum active surface, and the strong affinity between the support and the active materials could lead to good conductivity.[16, 17] Improved photothermal utilization and high-performance PTC activities can be expected for the Co_3O_4 catalysts grown on metal substrate with similar technique.

Specifically, herein we report ultrathin mesoporous Co_3O_4 nanosheets electrodeposited on stainless steel mesh (SS-Co_3O_4), which has never been used directly as a catalyst in gas-solid phase catalytic oxidation. Aerobic oxidations of propylene (C_3H_6) and propane (C_3H_8) under simulated sunlight were selected as probe reactions to explore the PTC activity. The structural superiority of SS-Co_3O_4 and the actual contribution of the SS substrate have been integrally discussed. It was found that the excellent PTC activity of SS-Co_3O_4 catalyst can be attributed to the maximum utilization of photothermal conversion, more catalytic active sites, and enhanced amount and mobility of surface lattice oxygen species. In addition, this work open new avenues towards the design of more energy-efficient monolith catalyst for the solar driven environmental purification.

2. Experimental

2.1 Catalysts preparation

Stainless steel mesh (SS, 200 mesh, 316 stainless steel, approximately 2 cm × 3 cm) was carefully cleaned with 2 M NaOH solution in an ultrasound bath for 30 min, and then rinsed with deionized water, acetone and absolute ethanol, respectively. SS-Co_3O_4 was synthesized through an electrochemistry deposition method as previously reported.[18] A standard three-electrode glass cell was used consisting of the clean SS working electrode, a platinum plate counter electrode and a saturated calomel reference electrode (SCE). The green $Co(OH)_2$ was electrodeposited upon SS in a 0.05 M $Co(NO_3)_2{\cdot}6H_2O$ aqueous electrolyte using A CHI 660C electrochemical workstation (Shanghai Chenhua, China). The electrodeposition potential is -1.0 V (vs. SCE). After electrodeposition for 20 min, the green stainless steel mesh was carefully rinsed several times with deionized water and dried at 60 ^{o}C, following by a calcination process at 250 ^{o}C for 2 h with a ramping rate of 1 ^{o}C min^{-1} to transform into Co_3O_4 nanosheets. In average, about 7 mg of Co_3O_4 nanosheets was grown on the 6 cm^2 SS (Table S1).

2.2 Characterization

The purity and crystallinity of the SS-Co_3O_4 was measured by X-ray diffraction (XRD) using a Rigaku D/MAX 2250 V diffractometer with monochromatized Cu Kα radiation (λ=0.15418 nm) under 40 kV, 100 mA and with the 2θ ranging from 10° to 80°. The morphologies and structures of the samples were characterized by scanning electron microscopy (SEM, Hitachi S-4800, Japan), transmission electron microscope (TEM), high-resolution transmission electron microscopy (HRTEM), selected area electron diffraction (SAED) (TecnaiG2 F20 S-Twin, accelerating voltage 200 kV), and N_2 adsorption-desorption measurements using a V-sorb 2800P surface area analyzer. The specific surface areas were calculated by the Brunauer–Emmett–Teller (BET) method. Pore volume and pore size distribution plots were obtained by the Barrett–Joyner–Halenda (BJH) method. X-ray photoelectron spectroscopy (XPS) were obtained by irradiating every sample with a 320 μm diameter spot of monochromated aluminum Kα X- rays at 1486.6 eV under ultrahigh vacuum conditions (performed on ESCALAB 250, THERMO SCIENTIFIC Ltd.). Charging effects were corrected by adjusting the binding energy of C 1s to 284.6 eV. UV-vis diffuse reflectance spectra (DRS) of the samples were measured using a Hitachi UV-3010PC UV-vis spectrophotometer. Oxygen temperature-programmed desorption (O_2-TPD) measurements were performed on a ChemiSorb 2750 instrument. Typically, 50 mg of the sample, placed in a glass tube, was pretreated by a He gas flow at 300 ^{o}C for 1 h. The adsorption of O_2 was then performed in a 4 vol% O_2/He gas flow for 1 h at room temperature. Afterward, the sample was heated to 900 ^{o}C at a rate of 10 ^{o}C min^{-1}. The TPD signal was recorded by a thermal conductivity detector. All the gas flow rates were set as 25 mL min^{-1}.

2.3 PTC oxidation of C_3H_6 and C_3H_8

The catalytic activities of all the samples were evaluated by the gas-phase aerobic oxidation of C_3H_6 (50 ppm) and C_3H_8 (50 ppm). The apparatus used was described in earlier papers.[19] Experiments were operated in a gas-closed vitreous reactor (capacity 600 mL) with a quartz window, and a 500 mW cm^{-2} Xe lamp was lighted to simulate the optical excitation and thermal activation. Before the catalytic test, a thermocouple was placed on the catalyst to measure the temperature of the catalyst under the irradiation of the Xe lamp. During the oxidation process, a GC analysis (GC 7900, Techcomp) equipped with two detective channels was used to detect the decrease of C_3H_6, C_3H_8 and the increase of CO_2 simultaneously. The channel for C_3H_6 and C_3H_8 detection consists of a TM plot-Al_2O_3/S capillary column and a flame ionization detector (FID). Another channel for CO_2 detection consists of a TDX-01, 80–100 mesh packed column followed by a methane conversion furnace and a FID.

2.4 TC oxidation of C_3H_8

The TC activities of SS-Co_3O_4 for C_3H_8 oxidation were tested in a quartz tube reactor with an inner diameter of 10mm at atmospheric pressure. The reagent gas consisted of 50 ppm C_3H_8 +20%O_2 + the balance made up of N_2 at a flow rate of 535 mL/min. 8 pieces of SS-Co_3O_4 were used as catalyst. The reactants and products were analyzed online by gas chromatograph (GC) equipped with a TCD.

3. Results and discussion

3.1 Structure and Morphology Analysis

SS-Co_3O_4 was synthesized through an electrochemistry deposition method. Its XRD pattern was readily indexed to a pure spinel phase of Co_3O_4 (JCPDS card no. 65-3103, Fig. S1 in supporting information (SI)). DTA/TG was performed to show the crystallization of Co_3O_4 (Fig. S2). The morphology and size of the as-prepared SS-Co_3O_4 was estimated by SEM. Fig. 1 shows the SEM images of the SS-Co_3O_4 with different magnifications. It can be clearly seen that uniform Co_3O_4 nanosheets with high density are well aligned on SS, which are interconnected to each other.[20] Especially concerning is that the thickness of every single Co_3O_4 nanosheet is estimated to be less than 10 nm (Fig. 1 C, D). More notably from the high resolution SEM image, the surface of every single Co_3O_4 nanosheet is full of voids, revealing that these nanosheets have foam-like porous inside architecture. These porous structures may be formed due to the dehydration and transformation of the crystalline structure during thermal treatment.[17] Thus, most of the nanosheet surface is highly accessible by the gaseous pollutant when used as a catalyst for VOCs disposal.

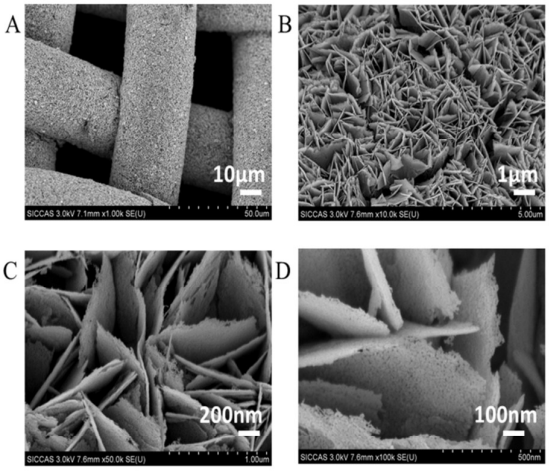

Fig. 1 SEM images of the Co_3O_4 nanosheet arrays supported on SS substrate (SS-Co_3O_4).

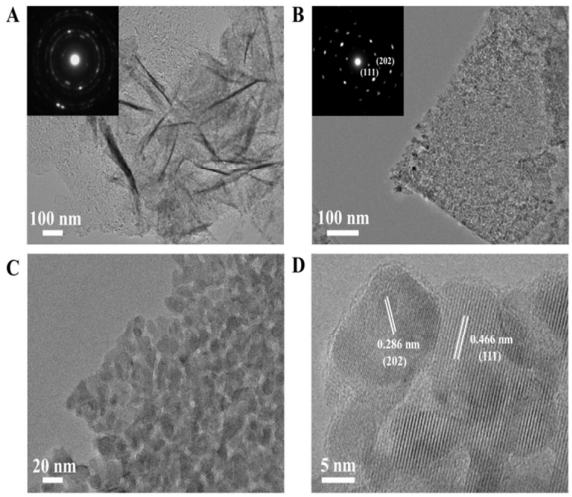

Fig. 2 (A)(B)TEM images and the insets in (A)(B) are SAED patterns, (C)(D) HRTEM images of the Co_3O_4 nanosheets scratched down from the SS substrate.

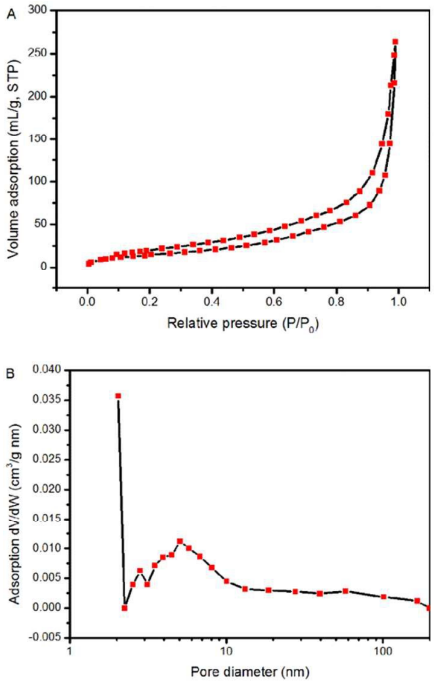

Fig. 3 (A) N_2 adsorption–desorption isotherms and (B) BJH desorption pore size distribution plots of the Co_3O_4 nanosheets scratched down from the SS substrate.

The structural feature of the SS-Co_3O_4 was further studied by TEM. Obviously, ultrathin feature of the Co_3O_4 nanosheet is further verified by the typical wrinkled structure of nanosheets observed in Fig. 2A.[21] Every ultrathin nanosheet consists of numerous interconnected nanoparticles with a size of *ca*. 10 nm forming a mesoporous structure (Fig. 2B, 2C). Furthermore, Fig. 3A, 3B proves that SS-Co_3O_4 have obvious porous foam-like inside architecture, which is well consistent with what we have observed from SEM. The lattice fringes in the HRTEM image (Fig. 2D) shows a well-defined crystalline structure with lattice spacings of 0.466 Å and 0.286 Å, corresponding to the value of the (111) and (202) planes of the

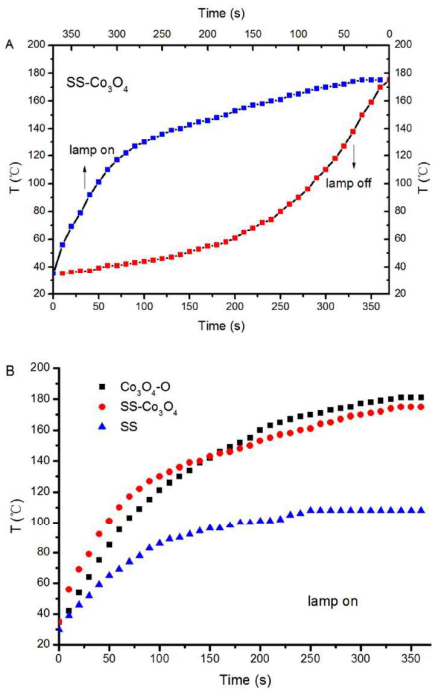

Fig. 4 Temporal change of the temperature on the catalysts under the irradiation of the Xe lamp.

Co_3O_4 phase. The SAED (inset of Fig. 2A, 2B) could be indexed as a polycrystalline pattern.

The Co_3O_4 nanosheets were scratched down from the SS through ultrasonication to estimate their mesoporosity and textural properties. From Fig. 3A, a typical IV isotherm (according to the IUPAC classification) with a distinct H3 hysteresis loop[22] in the pressure range of 0.6–1.0 P/P_0 can be clearly observed, suggesting the presence of a mesoporous structure of Co_3O_4 nanosheets.[23] Pore size distribution plot of the sample calculated by desorption isotherm via the BJH method (Fig. 3B) showed that pore size of Co_3O_4 nanosheets centered at around 6 nm, clarifying their mesoporosities. The BET specific surface area was measured to be 56.1 m^2g^{-1}.

3.2 Photothermal effect

For PC, it is a prerequisite for the catalysts to efficiently absorb solar light, and the infrared absorption ability is quite important for efficient photothermal conversion. For comparison, Co_3O_4-O (Co_3O_4 nanoparticles, SI) was prepared through an oxalate combustion method. We measured the UV-Vis-IR spectra of SS-Co_3O_4, Co_3O_4-O, and SS. Both SS-Co_3O_4 and Co_3O_4-O show strong absorption in the entire solar spectrum region with relatively weak absorption around 1000 nm (Fig. S3), while the former shows higher absorption than the latter in the presence of SS substrate.

Before the catalytic tests, the solar thermal effect was measured. For black Co_3O_4-O and SS-Co_3O_4 with good Vis–IR absorption (Fig. S3), strong solar heating can be expected. The temperature evolution profiles of Co_3O_4-O, SS-Co_3O_4, and pure SS under the irradiation of the Xe lamp are shown in Fig. 4 and Fig. S6. Impressively, the temperature of SS-Co_3O_4 quickly increases from room temperature to 110 °C in 60 s with the lamp on. When the temperature reaches a plateau, an equilibrium is established between the absorption of light energy and the energy dissipation from the catalyst to the surroundings.[24] The plateau temperatures (T_p) of Co_3O_4-O and SS-Co_3O_4 are 181 °C and 175 °C, revealing their efficient photothermal conversion. By comparing the temperature evolutions of the three in detail (Fig. 4B), apparently, SS-Co_3O_4 shows a little higher heating rate in 60 s but a little lower T_p than Co_3O_4-O. In view of the inefficient photothermal conversion of the pure SS (T_p 108 °C) and the low amount of Co_3O_4 nanosheets (only 7 mg on each SS), it can be concluded that SS-Co_3O_4 with its unique composition and structure is promising for utilizing IR energy as a mild heat source.

3.3 PTC Synergetic Activity

The light-off temperature (Ts) for C_3H_8 oxidation is significantly higher than for C_3H_6,[25, 26] which can be easily understood on the basis of the generally higher activity of alkenes compared to alkanes. The efficient PTC activity of SS-Co_3O_4 was investigated by evaluating the aerobic oxidation of C_3H_6 (50 ppm) and C_3H_8 (50 ppm) under the simulated solar irradiation of the Xe lamp. The C_3H_6 and C_3H_8 catalytic oxidation cannot proceed at room temperature without lighting. Besides, blank tests in the absence of any catalyst were performed (Fig. S7). The photolysis of C_3H_6 contributed to less than 11% of C_3H_6 decrease under a Xe lamp, while changes in C_3H_8 content were not distinct, indicating the indispensable role of the catalyst. The catalytic test with just a piece of SS in the reactor was also conducted. Apparently, pure SS did not show any catalytic activity towards the target gas (Fig. S7). The decrease in concentration (C_t/C_0) of the target gas (C_3H_6, C_3H_8) against the irradiation time over various catalysts are shown in Fig. 5A, 5B. A rapid decrease of both the C_3H_6 and C_3H_8 concentration was observed in the presence of SS-Co_3O_4 catalyst. About 90% C_3H_6 oxidation was achieved within 5 min, while 72% C_3H_8 oxidation was realized at the same time. Along with the fact that there are only 7 mg of Co_3O_4 nanosheets grown on the 6 cm^2 SS, it can be concluded that this novel SS-Co_3O_4 catalyst possesses superior PTC activity for both C_3H_6 and C_3H_8 oxidation. For comparison, we tested the catalytic activity of P25, TiO_2, and Co_3O_4-O (20 mg each) under the same experimental conditions. Also, 3 pieces of SS-Co_3O_4 (approximate 20 mg Co_3O_4) were used as catalyst. After the Xe lamp irradiation for 5 min, the C_3H_6 oxidation of Co_3O_4-O, P25 and TiO_2 is only 17.7%, 63%, and 50.7%, respectively. Meanwhile, with the same amount of catalyst, 82% C_3H_8 oxidation was achieved within 5 min for 3 pieces of SS-Co_3O_4, while no obvious change in C_3H_8 concentration can be seen for P25, TiO_2, and Co_3O_4-O. In general, SS-Co_3O_4 exhibit far better PTC activity in comparison to the behavior of the other three. The PTC durability test of SS-Co_3O_4 under the simulated solar irradiation was conducted, with each cycle lasting for 15 min.

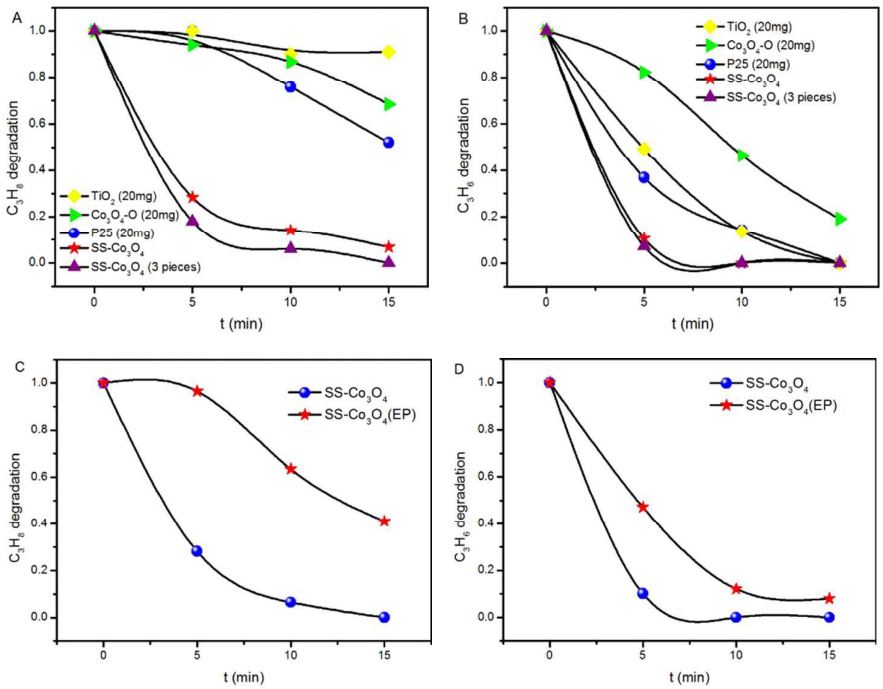

Fig. 5 (A)(B) C_3H_8 and C_3H_6 oxidation over SS-Co_3O_4, P25, TiO_2, and Co_3O_4-O under simulated sunlight (Xe lamp). (C)(D) C_3H_8 and C_3H_6 oxidation over SS-Co_3O_4 and SS-Co_3O_4(EP) under simulated sunlight (Xe lamp).

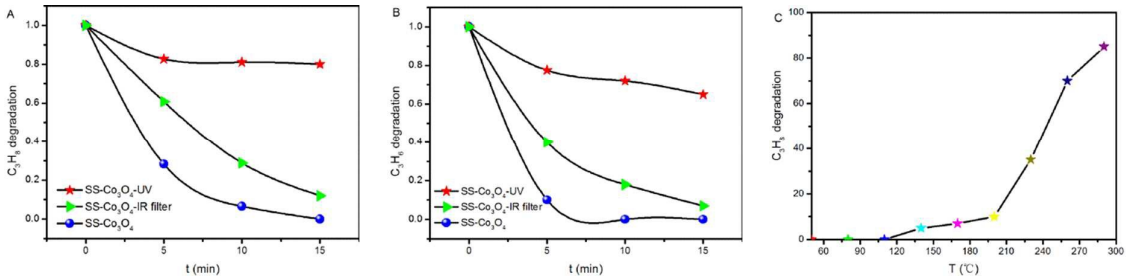

Fig. 6 (A)(B) C_3H_8 and C_3H_6 oxidation over SS-Co_3O_4 under simulated sunlight, UV light, and infrared light. (C) Thermocatalytic performance of SS-Co_3O_4 for C_3H_8 oxidation.

Take the PTC oxidation of C_3H_8 as an example, as it shown in Fig. S8, despite some minor fluctuations, the C_3H_8 conversion ratio basically keeps above 90%, indicating an excellent catalytic durability.

To further emphasize the structural superiority of SS-Co_3O_4 and to identify the possible contribution of the metal substrate, Co_3O_4-O was deposited on SS with the same area using electrophoresis technology. The resulting sample was denoted as SS-Co_3O_4 (EP) and used to test the PTC activity. From Fig. 5C, 5D, about 3.5% C_3H_8 oxidation and 52.9% C_3H_6 oxidation of SS-Co_3O_4 (EP) are achieved within 5 min, which is much lower than that of the SS-Co_3O_4 catalyst. Integrate the behavior of SS, SS-Co_3O_4, SS-Co_3O_4 (EP) and Co_3O_4-O, it can be derived that 1) the excellent PTC activity merely occurs around the direct grown SS-Co_3O_4 rather than the Co_3O_4 coated SS; 2) a synergetic interaction between the SS substrate and the Co_3O_4 nanosheets has enabled the superior performance. Detailed analysis will be in the mechanism section.

We tested the catalytic activity of the SS-Co_3O_4 under the infrared irradiation of the Xe lamp by using cutoff filter to filter out the wavelengths below 690 nm, and also under the irradiation of a UV lamp (15W). It can be seen from Fig. 6A, 6B that SS-Co_3O_4 exhibits efficient infrared-light driven catalytic activity for oxidation of target gas. Specifically, about 39.2% C_3H_8 oxidation and 60% C_3H_6 oxidation were achieved within 5 min, which accounted for nearly 60% of the catalytic activities under the full solar spectrum Xe lamp irradiation. The red dots in Fig. 6A, 6B showed results using a UV lamp as light source. The UV part could only show a slight contribution, giving oxidation ratio of 17.3%, 22.5% within 5 min for C_3H_6 and C_3H_8, respectively, with the results remained almost unchanged for the next 10 min. Moreover, as the oxidation of C_3H_8 was much more difficult than that of C_3H_6, C_3H_8 was chosen in the individual TC oxidation tests to determine the temperature at which the catalytic activity of SS-Co_3O_4 starts (T_s). Impressively, C_3H_8 oxidation starts at around 100 °C (T_s, Fig. 6C), which is much lower than the corresponding T_p (175 °C) of SS-Co_3O_4

under the Xe lamp irradiation. Thus, the high T_p induced by efficient photothermal conversion is enough to trigger off TC C_3H_8 oxidation for SS-Co_3O_4 in the Xe lamp irradiation experiments. Hou *et al.*[24] demonstrated a novel Ce ion substituted OMS-2 catalyst, which can efficiently transform the absorbed solar energy to thermal energy, and a mechanism of solar light driven TC was proposed. For the SS-Co_3O_4 catalyst in this study, not only the solar light driven TC existed, but also PC oxidation was present with the Xe lamp on. Recent studies[7, 27] have shown a synergetic effect between the PC and the TC oxidation does exist, resulting in excellent PTC oxidation activity.

3.4 Mechanism

The question is why the SS-Co_3O_4 with small amounts of Co_3O_4 on the SS substrate exhibits highly efficient PTC activity for the catalytic oxidation of light hydrocarbons. In this section, the origins of the excellent PTC activity of Co_3O_4 are discussed in detail.

3.4.1 Metal substrate-enhanced photothermal conversion

Results in Fig. 5 clearly indicate that the SS-Co_3O_4 catalyst with low growth amount of Co_3O_4 nanosheets, possesses superior PTC activity for both C_3H_6 and C_3H_8 oxidation. The excellent PTC activity merely occurs around the direct grown SS-Co_3O_4 rather than the Co_3O_4-O coated SS or Co_3O_4 nanoparticles, notwithstanding the bigger BET specific surface area and higher T_p of Co_3O_4-O (SI). Remembering of the higher heating rate in 60s and the just little lower T_p of SS-Co_3O_4 in Fig. 4, it can be concluded that the substrate SS plays an important role in the PTC process. SS-Co_3O_4 realizes much stronger photoabsorption abilities and greater instant photoresponse than Co_3O_4 nanoparticles (Fig. S3, Fig. S9), both of which favor photothermal conversion. The enhanced PTC process by substrate SS has been explained by the following events: First, due to the low heat capacity of the metal substrate (i.e., high heating rate), it is much more easily to achieve the light-off temperature of the catalyst. And with good thermal conductivity and fast heat transfer property, SS substrate can effectively prevent the overheating induced deactivation of the catalyst. Different substrates (nickel foam, FTO conducting glass and SS, 2 cm × 3 cm) were chosen for the preparation of Co_3O_4 using the same electrochemistry deposition method (Fig. S10). Generally, thermal conductivity coefficient (λ) of nickel foam is a bit higher than SS, and λ of FTO is two orders of magnitude lower than nickel foam and SS. Obviously, Ni-Co_3O_4 shows the highest catalytic activity, while nearly no change in C_3H_8 and C_3H_6 concentration can be seen for FTO-Co_3O_4. Besides, without substrate, the Co_3O_4 nanosheets show good PTC activity towards C_3H_8 and C_3H_6 oxidation, but much lower than that of Ni-Co_3O_4 and SS-Co_3O_4, further confirms the importance of the substrate. Second, the SS can provide a stable framework and hierarchical porous channels to ensure efficient contact between the surface of Co_3O_4 nanosheets and the gaseous pollutants, which increase the surface exposed catalytic-active species for catalytic reactions. Such a structure could also shorten the electron transfer distance,[18, 28] thus greatly reducing the probability of the recombination of the photoinduced electron and hole.[29] Furthermore, the foam-like porous inside architecture of Co_3O_4 nanosheets possesses more active sites and is favor of light harvesting.

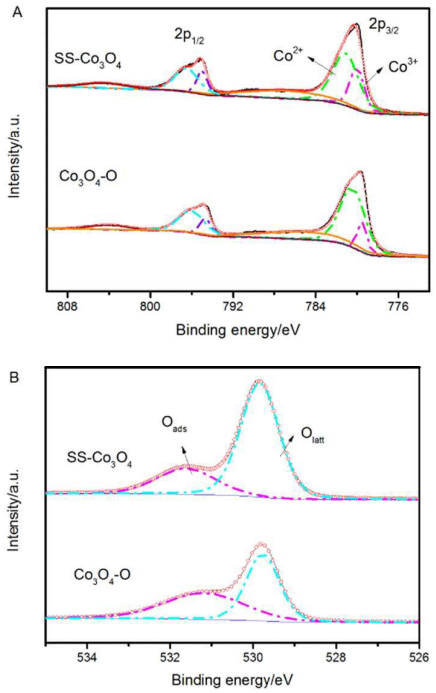

Fig. 7 (A) Co 2p XPS spectra and (B) O 1s XPS spectra of SS-Co_3O_4 and Co_3O_4-O.

Table 1. Summary of area percentages of different elemental components obtained from the deconvoluted spectra

sample	% area			
	Co $2p_{3/2}$		O 1s	
	Co^{3+}	Co^{2+}	O_{latt}	O_{ads}
SS-Co_3O_4	20.4	46.2	73.8	26.2
Co_3O_4-O	11.9	54.7	50.9	49.1

3.4.2 Higher Co^{3+} content

Specifically, the catalytic activity is thought to be related to the reducibility of the active sites for the deep oxidation of light hydrocarbons.[30] XPS was performed to further investigate the surface compositions and elementary oxidation states. The XPS spectra of Co 2p and O 1s for Co_3O_4-O and SS-Co_3O_4 are displayed in Fig. 7. Generally, in Co 2p XPS spectra, the bands at *ca.* 795.9 eV (Co $2p_{1/2}$) and *ca.* 780.9 eV (Co $2p_{3/2}$) were indicative of Co^{2+} chemical state whilst the bands at *ca.* 794.6 eV (Co $2p_{1/2}$) and *ca.* 779.5 eV (Co $2p_{3/2}$) were corresponded to Co^{3+}.[31] Here, the spin-orbit splitting value of Co 2p for SS-

Co_3O_4 is 15.2±0.1 eV, which is close to that of mixed-valence Co_3O_4, so the cobalt species of SS- Co_3O_4 is Co_3O_4.[10] Different surface oxygen species have been identified by the deconvoluted O 1s spectrum. Fig. 7B revealed the fitted O1s peaks of lattice oxygen species (O^{2-}, denoted as O_{latt}) at 530.1–530.2 eV, chemisorbed oxygen species (O^- and O_2^-, denoted as O_{ads}) at 531.2–531.3eV in each sample.[2] Peak area percentages of different Co and O components are listed in table 1. The Co^{3+}/Co^{2+} ratios of Co_3O_4-O and SS-Co_3O_4 were calculated to be 0.22 and 0.44, among which SS-Co_3O_4 had higher amount of Co^{3+} and exhibited more abundant lattice oxygen species on the surface.

Co^{3+} is generally considered to be the catalytic active site of Co_3O_4. The relative surface content of Co^{3+} cations played a very important role in the catalytic activities of Co_3O_4.[32] A breakthrough on Co_3O_4 for catalytic CO oxidation showing that Co_3O_4 nanorods with four {110} surface planes exhibit a much higher catalytic activity for CO oxidation and larger resistance to deactivation by water than Co_3O_4 nanoparticles was reported by Xie *et al*.[33] The high catalytic activity of Co_3O_4 {110} planes is attributed to its higher concentration of Co^{3+} cations (correspondingly fewer Co^{2+} cations) than other crystal planes, since only Co^{3+} cations surrounded by Co^{2+} ions are active for catalytic oxidation of CO.[34] It has also been observed that that the variation of the catalytic activity of Co_3O_4/ZSM-5 catalysts for propane oxidation parallels both the relative content of surface Co^{3+} and the reducibility of Co^{3+}.[30] Hence, the obtained ultrahigh PTC activity of the SS-Co_3O_4 was in part because of the abundance of active Co^{3+} on the surface.

3.4.3 Surface lattice oxygen

To get insight into the adsorption and activation of oxygen on SS-Co_3O_4, and further investigate the lattice oxygen mobility of the catalyst, O_2-TPD analysis was performed. It is well known that the surface adsorbed oxygen species changes by the following procedures:[35] O_2(ad) →O_2^- (ad)→O^- (ad)→O^{2-} (ad/lattice). O_2(ad) refers to physically adsorbed oxygen, which can usually be removed by purging helium before the analysis. The oxygen adsorbed species of O_2^- (ad) and O^- (ad) are located at surface vacancies and are easier to desorb. O^{2-} (ad/lattice) is the surface lattice oxygen and is difficult to be extracted.[36] On the basis of results from the literature,[37] the oxygen desorption peaks of Co_3O_4 with respect to temperature ranges can be classified as follows:[38]

(1) 100–200 °C: desorption of surface adsorbed peroxy species O_2^- (ad),

(2) 200–400 °C: desorption of surface adsorbed monatomic species O^- (ad),

(3) 400–700 °C: desorption of surface lattice oxygen O^{2-} (ad/lattice), and

(4) Beyond 700 °C: desorption of bulk lattice oxygen

From Fig. 8, it can be seen that the Co_3O_4 nanosheets scratched down from the SS foam (red line) did not show obvious O_2^- (ad) desorption peak in the temperature range of 100–200 °C, where the Co_3O_4-O sample (black line) revealed the distinct O_2^- (ad) desorption peak. O^- (ad) desorption peak

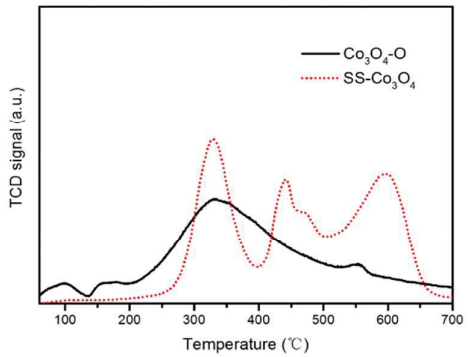

Fig. 8 O_2-TPD profiles of the Co_3O_4-O nanoparticles and the Co_3O_4 nanosheets scratched down from the SS substrate.

of the two samples located almost at the same temperature. Notably, for the O^{2-} (ad/lattice) desorption, SS-Co_3O_4 revealed a much lower temperature and much wider range, indicating that the desorption amount and the mobility of surface lattice oxygen species of SS-Co_3O_4 catalyst is greatly enhanced in comparison with Co_3O_4-O nanoparticles. It has been widely accepted that VOCs oxidation over metal oxides follows a mechanism developed by Mars-van and Krevelen involving the participation of a lattice oxygen by a redox cycle.[39] Lattice oxygen can be both the adsorption site and active site of the catalyst for VOCs catalytic oxidation.[40] In the research of Finocchio,[26] the experimental data strongly support a typical Mars-van Krevelen type mechanism for C_3H_8 and C_3H_6 catalytic combustion over Co_3O_4 catalysts where the oxidizing center is, accordingly, Co^{3+} and the active oxygen species is nucleophilic O^{2-} (ad/lattice) at the oxidized surface. For the combustion of methane over the cobalt oxide catalyst, it also follows a Mars–Van Krevelen mechanism and depends on the fast migration of oxygen ions through the lattice of cobalt oxide.[41] Herein, the amount and mobility of surface lattice oxygen is a significant factor to sustain the much higher catalytic activity of the SS-Co_3O_4.

On the basis of the above discussion of a series of critical factors for the PTC oxidation process, it can be concluded that the combined properties of SS-Co_3O_4 such as ultrathin two-dimension shape, foam-like porous inside architecture, and supported metal substrate could lead to integrative advantages of the maximum utilization of photothermal conversion, more catalytic active sites, and enhanced amount and mobility of surface lattice oxygen species, resulting in the excellent PTC activity of SS-Co_3O_4 catalyst.

4. Conclusions

In summary, ultrathin mesoporous Co_3O_4 nanosheets on stainless steel mesh (SS-Co_3O_4) have been synthesized through an electrochemistry deposition method. The SS-Co_3O_4 catalyst exhibits strong absorption in the entire solar spectrum and shows strong solar heating effect, resulting in a considerable increase of temperature above the light-off temperature for

VOCs oxidation. Aerobic oxidations of C_3H_6 and C_3H_8 under simulated sunlight, UV light, and infrared light irradiation were performed. This novel SS-Co_3O_4 catalyst with only 7 mg of Co_3O_4 grown possesses superior PTC activity, much better than the P25, TiO_2, and Co_3O_4 nanoparticles. The structural superiority of SS-Co_3O_4 and the actual contribution of the metal substrate to the PTC process have been integrally discussed. The C_3H_6 and C_3H_8 oxidation over SS-Co_3O_4 follows the Mars-van Krevelen redox mechanism. The excellent PTC activity of SS-Co_3O_4 catalyst can be attributed to the maximum utilization of photothermal conversion, more catalytic active sites, and enhanced amount and mobility of surface lattice oxygen species. On the basis of this study, a brand new strategy for catalyst design toward the fully use of both the light and heat of the solar energy is suggested. In addition, the system of metal substrate supported ultrathin cobalt oxide nanosheets could be of interest as a monolith catalyst in many practical applications.

Acknowledgements

We acknowledge the financial support from the National Basic Research Program of China (2013CB933203), National Natural Science Foundation of China (51272269, 51272303, and 51472260).

Notes and references

1 P. Christopher, H. L. Xin and S. Linic, *Nature chemistry*, 2011, **3**, 467-472.
2 B. Bai and J. Li, *ACS Catal.*, 2014, **4**, 2753-2762.
3 J. H.W. Prengle and W. E. Wentworth, University of Houston, 1992.
4 T. T. Trinh, R. Sato, M. Sakamoto, Y. Fujiyoshi, M. Haruta, H. Kurata and T. Teranishi, *Nanoscale*, 2015, **7**, 12435-12444.
5 Z. Wang, C. Yang, T. Lin, H. Yin, P. Chen, D. Wan, F. Xu, F. Huang, J. Lin, X. Xie and M. Jiang, *Energ. Environ. Sci.,* 2013, **6**, 3007.
6 Y. H. Qu, F. Liu, Y. Wei, C. L. Gu, L. H. Zhang and Y. Liu, *Appl. Surf. Sci.*, 2015, **343**, 207-211.
7 W. Xie, Y. Z. Li, W. Q. Shi, L. Zhao, X. J. Zhao, P. F. Fang, F. Zheng and S. J. Wang, *Chem. Eng. J.*, 2012, **213**, 218-224.
8 Y. Li, Q. Sun, M. Kong, W. Shi, J. Huang, J. Tang and X. Zhao, *J. Phys. Chem. C*, 2011, **115**, 14050-14057.
9 J. L. Falconer and K. A. Magrini-Bair, *J. Catal.*, 1998, **179**, 171-178.
10 Y. Zheng, W. Wang, D. Jiang and L. Zhang, *Chem. Eng. J.*, 2016, **284**, 21-27.
11 D. Jiang, W. Wang, E. Gao, L. Zhang and S. Sun, *J. Phys. Chem. C*, 2013, **117**, 24242-24249.
12 H. Yang, G. Zhu, D. Zhang, D. Xu and S. Qiu, *Microporous Mesoporous Mater.*, 2007, **102**, 95-100.
13 J. R. Adleman, D. A. Boyd, D. G. Goodwin and D. Psaltis, *Nano lett.*, 2009, **9**, 4417-4423.
14 M. Haneda, Y. Kintaichi, N. Bion and H. Hamada, *Appl. Catal. B: Environ.*, 2003, **46**, 473-482.
15 L. F. Liotta, H. Wu, G. Pantaleo and A. M. Venezia, *Catal. Sci. Technol.*, 2013, **3**, 3085.
16 Y. Fan, N. Zhang, L. Zhang, H. Shao, J. Wang, J. Zhang and C. Cao, *J. Electrochem. Soc.*, 2013, **160**, F218-F223.
17 Y. Fan, H. Shao, J. Wang, L. Liu, J. Zhang and C. Cao, *Chem. Commun.* , 2011, **47**, 3469-3471.
18 C. Yuan, L. Yang, L. Hou, L. Shen, X. Zhang and X. W. Lou, *Energ. Environ. Sci.*, 2012, **5**, 7883.
19 D. Jiang, W. Wang, S. Sun, L. Zhang and Y. Zheng, *ACS Catal.*, 2015, **5**, 613-621.
20 C. Cheng, G. Zhou, J. Du, H. Zhang, D. Guo, Q. Li, W. Wei and L. Chen, *New J Chem.*, 2014, **38**, 2250-2253.
21 J. Bao, X. Zhang, B. Fan, J. Zhang, M. Zhou, W. Yang, X. Hu, H. Wang, B. Pan and Y. Xie, *Angew. Chem. Int. Ed.*, 2015, **54**, 7399-7404.
22 M. Roy, S. Ghosh and M. K. Naskar, *Phys. Chem. Chem. Phys.,* 2015, **17**, 10160-10169.
23 C. Santra, S. Rahman, S. Bojja, O. O. James, D. Sen, S. Maity, A. K. Mohanty, S. Mazumder and B. Chowdhury, *Catal.Sci. Technol.*, 2013, **3**, 360-370.
24 J. Hou, Y. Li, M. Mao, Y. Yue, G. N. Greaves and X. Zhao, *Nanoscale*, 2015, **7**, 2633-2640.
25 A. C. Gluhoi, N. Bogdanchikova and B. E. Nieuwenhuys, *Catal. Today*, 2006, **113**, 178-181.
26 Elisabetta Finocchio, Guido Busca, Vincenzo Lorenzelli and V. S. Escribanob, *J. Chem. Soc., Faraday Trans.*, 1996, **9**, 1587-1593
27 S. Kohtani, K. Yoshida, T. Maekawa, A. Iwase, A. Kudo, H. Miyabe and R. Nakagaki, *Phys. Chem. Chem. Phys.*, 2008, **10**, 2986-2992.
28 Y. Fan, G. Shao, Z. Ma, G. Wang, H. Shao and S. Yan, *Part. Part. Syst. Char.* , 2014, **31**, 1079-1083.
29 Q. Shen, Z. Chen, X. Huang, M. Liu and G. Zhao, *Environ. Sci. Technol.*, 2015, **49**, 5828-5835.
30 Z. Zhu, G. Lu, Z. Zhang, Y. Guo, Y. Guo and Y. Wang, *ACS Catal.* , 2013, 1154-1164.
31 A. Y. Khodakov, W. Chu and P. Fongarland, *Chem. Rev.*, 2007, **107**, 1692-1744.
32 Y. Sun, P. Lv, J. Y. Yang, L. He, J. C. Nie, X. Liu and Y. Li, *Chem. Commun.*, 2011, **47**, 11279-11281.
33 X. Xie, Y. Li, Z.-Q. Liu, M. Haruta and W. Shen, *Nature*, 2009, **458**, 746-749.
34 M. Zhou, L. Cai, M. Bajdich, M. García-Melchor, H. Li, J. He, J. Wilcox, W. Wu, A. Vojvodic and X. Zheng, *ACS Catal.*, 2015, **5**, 4485-4491.
35 A. Bielański and J. Haber, *Cat. Rev.*, 1979, **19**, 1-41.
36 C. S. Deng, B. Li, L. H. Dong, F. Y. Zhang, M. G. Fan, G. Z. Jin, J. B. Gao, L. L.Gao, Z. G. Fei and X. Zhou, *Phys. Chem. Chem. Phys.*, 2015, **17**, 16092--16109.
37 K. B. Sravan Kumar and P. A. Deshpande, *J. Phys. Chem. C*, 2015, **119**, 8692-8702.
38 W. Song, A. S. Poyraz, Y. Meng, Z. Ren, S.-Y. Chen and S. L. Suib, *Chem. Mater.* , 2014, **26**, 4629-4639.
39 B. Solsona, T. E. Davies, T. Garcia, I. Vázquez, A. Dejoz and S. H. Taylor, *Appl. Catal. B: Environ.*, 2008, **84**, 176-184.
40 H. Sun, Z. Liu, S. Chen and X. Quan, *Chem. Eng. J.*, 2015, **270**, 58-65.
41 N. Bahlawane, *Appl. Catal. B: Environ.*, 2006, **67**, 168-176.

Graphical Abstract

□ Ultrathin mesoporous Co_3O_4 nanosheets electrodeposited on stainless steel mesh (SS-Co_3O_4) exhibit high photothermal performance and possess superior PTC activity.